УДК 538.245

THERMOCONTROLLED MAGNETIC MATERIALS FOR MEMS (review)

M. S. Kustov[1], G. A. Lebedev[2], S. E. Ilyashenko[3], D. V. Druina[1], O. V. Gasanov[1], S. A. Chigirinsky[4], O. M. Korpusov[5], A. B. Zalyotov[5], R. M. Grechishkin[1]

[1] Tver State University, *Laboratory of Magnetoelectronics*
[2] CEA, LETI, MINATEC Campus, Grenoble, France
[3] Tver State Technical University
[4] OSTEC Ltd, Moscow
[5] Tver State Medical Academy

Three novel types of magnetic materials (thermoreversible permanent magnets, spin-reorientation compounds and ferromagnetically ordered Heusler-type shape memory alloys) which show promise for future applications related to microelectromechanical systems (MEMS) are reviewed. The role of magnetic domain structure (DS) observations in understanding the magnetic behaviour of these materials is emphasized. The magnetic properties and DS of high-coercivity ferrimagnetic $GdCo_{5-x}Cu_x$ alloys exhibiting the effect of Gd- and 3*d*-sublattice magnetization compensation at defined temperatures are described with respect to their use as thermo-reversible permanent magnets. Changes in the DS type during the spin-reorientation transition from the easy axis to the easy plane state are shown for the example of $DyCo_5$ intermetallic compound. Magnetically ordered Heusler-type shape memory alloys (Ni-Mn-Ga, Co-Ni-Ga) are characterized by the cooperation of the martensitic and magnetic DS. Examples of possible applications of these three materials in MEMS-related devices are given.

Keywords: *thermoreversible magnets, hard magnetic materials, rare earth compounds, spin reorientation, shape memory alloys, magnetic domain structure, magnetooptic imaging films*

1. Introduction. Development of less-common magnetic materials and understanding of their behaviour in different external conditions is at the root of progress in many areas of materials science [1–4]. This is particularly true in the development of magnetic materials for a variety of important applications related to microelectromechanical systems (MEMS) [5]. On one hand, MEMS devices borrow from integrated circuit manufacturing, so some of the existing technologies of preparing bulk magnetic materials should be modified to satisfy new requirements. On the other hand, new possibilities coming from miniaturization and integration of MEMS with optical, electronic, magnetic, and thermal functional devices make it possible to realize operational principles, the implementation of which was impractical or impossible with the traditional macrosystems. From this point of view it

may be expected that at least some of the more unusual materials and effects will find use in MEMS in the near future.

In the present article we focus our attention on three types of less-common magnetic materials – (*i*) thermoreversible permanent magnets, (*ii*) spin-reorientation materials, and (*iii*) ferromagnetic shape memory alloys which we are presently xstudying for their potential application in MEMS. Due to some specific features of these materials their simple classification on the basis of magnetic hardness, softness or magnetostriction is insufficient, so more detailed understanding of their properties is necessary. In the present work, alongside traditional methods of magnetic characterization, we place an emphasis on the observation of magnetic DS providing important information on the magnetic behavior of materials.

2. Thermoreversible permanent magnets

2.1. Preamble. Permanent magnets (PM) are used as a source of magnetic flux in a wide range of applications [6]. In general, in most cases it is required that the magnetic properties of the magnet (remanence and coercivity) are stable over the working temperature range. On the contrary, here we demonstrate the exploitation of the thermal variation of the magnetic properties of ferrimagnetic alloys with a compensation temperature [7]. In this study we demonstrate that the substitution of appropriate amounts of Cu for Co in $Gd(Co_{5-x}Cu_x)$ leads to the development of significant values of coercivity over a useful temperature range, rendering it a permanent magnet.

In rare earth transition metal intermetallics (R–TM) the coupling between the rare-earth moment, $\mu_R = g\mu_B m_J$ (g – Lande factor, μ_B – Bohr magneton, m_J – angular moment), and that of the transition metal species, $\mu_{TM} = g\mu_B m_s$ (m_s – spin moment), is ferromagnetic for light rare-earth ($\mathbf{J} - \mathbf{s} > 0$) and antiferromagnetic for heavy rare-earths ($\mathbf{J} - \mathbf{s} < 0$) [7]. In the first half of a shell, according to Hund's rule, $J = L - S$ (total moment and spin moments are antiparallel), while in the second half $J = L + S$, so the spin-spin coupling between R and TM species is always antiferromagnetic (Fig. 1).

The temperature dependence of spontaneous magnetization of ferrimagnets is determined by the magnetic moments and temperature dependence of the sublattices as described by Neel's theory of ferrimagnetism [7]. For binary $GdCo_5$ of the 1:5 stoichiometry, as well as for $GdCo_3$ and $GdCo_4$, a compensation point exists in the temperature dependence of the magnetization. Substitution of Co for other 3*d*-transition elements results in a change (decrease) of the Co sublattice magnetic moment because of dilution and also due to filling of the Co 3*d*-band by valence electrons.

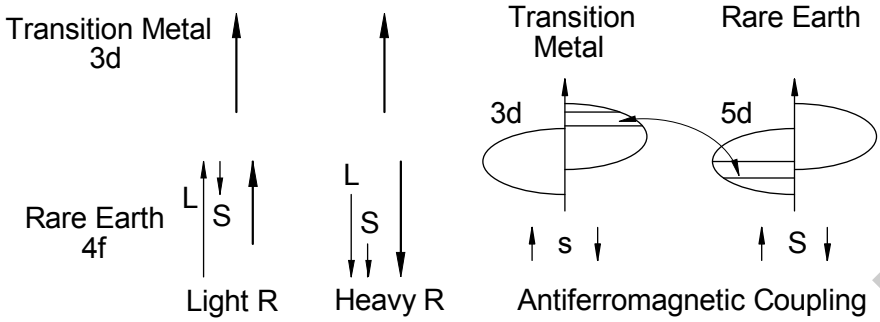

Fig. 1. Schematic representation of spin and angular momentum coupling at rare earth site and antiferromagnetic exchange coupling between R and TM spins

The role of a third, 3*d*-transition element, such as Cu, Al, Ni or Fe in modifying the coercivity of rare-earth cobalt alloys has been the subject of a number of studies. In particular, it was demonstrated that Cu and Ni substitutions in the quasibinary $Sm(Co_{5-x}M_x)$ system may lead to giant magnetic hardness combined with giant magnetic viscosity [8–11]. Al and Fe replacements were shown to be useful in regulating the easy plane – easy axis spin reorientation temperature region in quaternary $Nd(Co_{1-x-y}Al_xFe_y)_5$ soft magnetic alloys applicable in thermal sensors and actuators [12], while Ni substitutions for Co provided an effective control of the compensation temperature in ferrimagnetic Gd-Co-Ni films [13].

In the present study we investigated the ferrimagnetic quasibinary $Gd(Co_{5-x}Cu_x)$ system in the expectation that Cu substitution will, by analogy with $Sm(Co_{5-x}Cu_x)$ compounds, increase the coercive force of the magnetically soft binary $GdCo_5$ to values typical of PM, retaining at the same time the phenomena of reversible macroscopic compensation of the material's magnetization at some predetermined temperature.

2.2. Experimental. Coarse-grained (average grain size 2…4 mm) 50 g ingots were prepared by induction melting in alumina crucibles of Gd, Co (both of 99.8% purity) and Cu (99.99%). The ingots were vacuum annealed at 1273 K for 2 hours and then cooled to room temperature (RT) at a rate of 100 K/min. No attempts were made for special heat treatments which possibly will be useful in maximizing the coercive field. Spherical single crystal samples (diameter ~2 mm) were ground from selected large grains. Hysteresis loops were measured using an automated VSM in an electromagnet with a maximum field of 3 T. Magneto-optic indicator films (MOIF) [14] were used to visualize the stray fields and magnetic DS of the samples.

2.3. Results and discussion. Shown in Fig. 2 are the RT values of the saturation magnetization and coercive field for $GdCo_{5-x}Cu_x$ ($x = 0…2.5$) samples as a function of composition. It is seen that the RT value of the

compensation point and the maximum measured value of H_c occur at $x \approx 1.5$; coercive fields for the practically interesting temperature interval in the vicinity of RT are much greater than in the binary $GdCo_5$ ($x = 0$, $\mu_0 H_c \approx 30$ mT), varying between 0.3…1.6 T within the range $x = 1…2.2$.

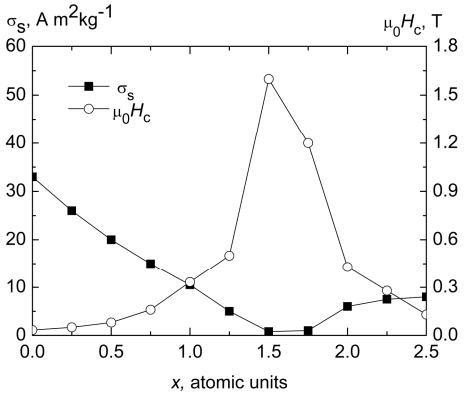

Fig. 2. Specific saturation magnetization σ_S and coercive field $\mu_0 H_C$ of ferrimagnetic $GdCo_{5-x}Cu_x$ ($x = 0...2.5$) single crystals as a function of composition

Fig. 3 presents the room temperature major hysteresis loops of electropolished single crystals for the cobalt-rich part of the $GdCo_{5-x}Cu_x$ system ($x = 0.25…1.25$) measured after saturation in fields of ±2 T (shown in the graph are the central parts limited to ±0.8 T). These loops demonstrate 100% remanence and ideal rectangularity similar to those observed earlier in binary alloys [15, 16]. In non-polished polycrystalline samples the remanence and loop rectangularity depend on the degree of texture; the coercive field values, however, are the same or higher than in single crystals. The coercive field H_c increases and the saturation magnetization σ_s decreases as x approaches the compensation composition ($x = 1.5$). The behavior is reversed as x increases above this value (full hysteresis loops not shown for clarity).

Shown in Fig. 4 are the initial curves of magnetization for the same samples. It is seen that for binary $GdCo_5$ magnetic saturation is easily achieved in a field of about 0.1 T, corresponding to the demagnetizing field of a sphere (demagnetizing factor 0.33), as should be expected for a low-coercive material. Different behaviour is observed for quasibinary alloys: here the ascending part of the magnetization curve shifts to higher fields with the increase of Cu content.

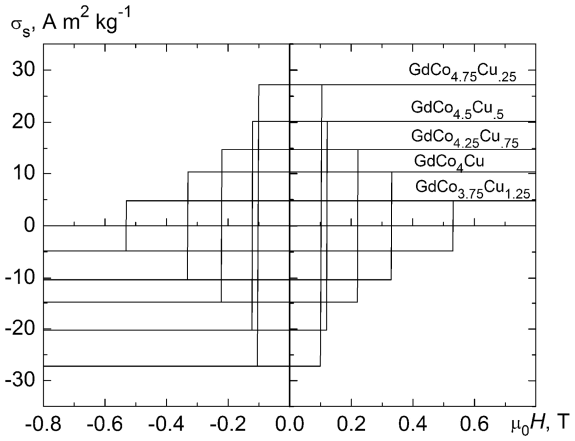

Fig. 3. Easy axis major hysteresis loops of electropolished spherical single crystals of $GdCo_{5-x}Cu_x$ (x = 0.25…1.25)

Moreover, these parts of the curves are characterized by large magnetic aftereffect (magnetic viscosity) with relaxation times (depending on the external field value) up to 10^3…10^4 seconds. These features are typical for high-coercive materials reversing magnetization by the pinning-controlled motion of domain walls [6–11].

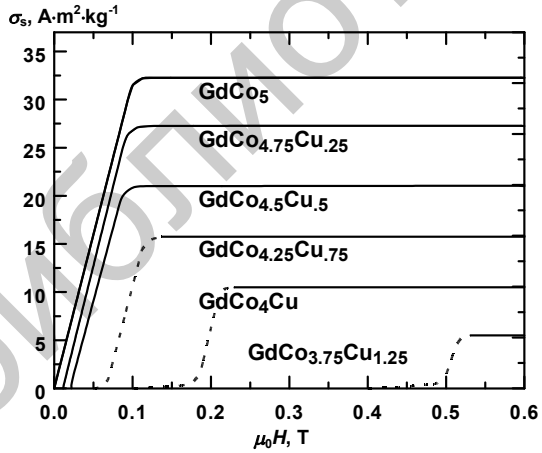

Fig. 4. Initial magnetization curves for $GdCo_{5-x}Cu_x$ alloys along the easy magnetization direction. Dashed lines correspond to regions of magnetic superviscosity

Fig. 5 shows the whole family of minor and major hysteresis loops for $GdCo_4Cu$ crystal with moderate Cu content (x = 1). It is seen that for the inner group of loops the coercive field is practically independent of the magnetizing field. This is a typical attribute of pinning-controlled reversal. On the contrary, for the outward group the field of the jump-like reversal process depends in a stepwise manner on the magnetizing field resulting in a series of ideally rectangular loops characteristic of a nucleation-controlled

mechanism [17]. Thus Fig. 5 demonstrates two separated magnetization reversal mechanisms coexisting in the same sample.

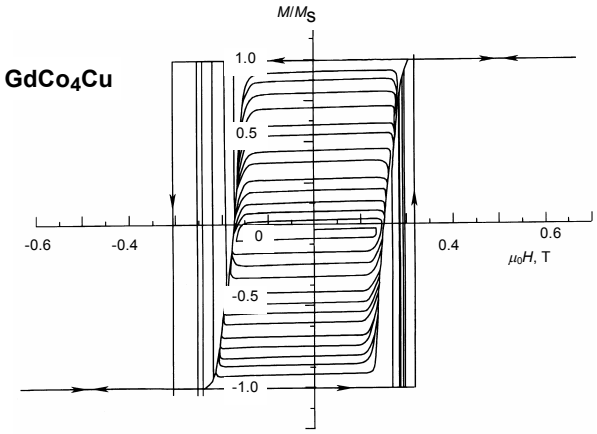

F i g . 5. Hysteresis loop family for GdCo4Cu single crystal

Fig. 6 illustrates the magnetization reversal process of the $GdCo_3Cu_2$ disk-shaped (diameter 2 mm) sample observed with the aid of MOIF [14]. Remanent DS of the sample initially saturated in the positive direction normal to the surface was observed under the action of negative pulses (duration 20 μs) of progressively increasing amplitude. It is seen that the applied technique of observation provides reliable and pictorial information on the magnetic state of the sample consistent with other measurements.

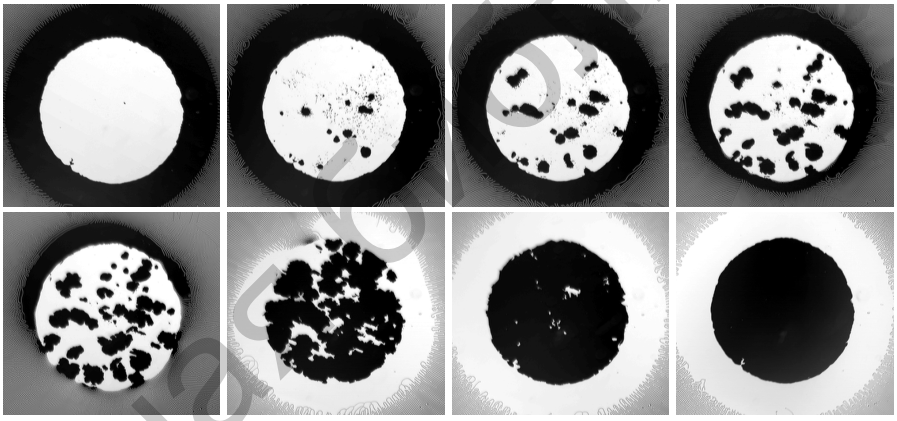

F i g . 6. Magnetization reversal from $+M_r$ to $-M_r$ of GdCo3Cu2 under the action of negative field pulses of progressively increasing magnitude

This method of observation was further applied to examine the process of temperature driven magnetization inversion on passing through the ferrimagnetic compensation point of the alloys under study.

The images presented in Fig. 7 show the distribution of the normal component of the field at the surface of the $GdCo_3Cu_2$ sample magnetized to saturation. The sample, in the shape of a thin disk with a diameter of 2 mm and thickness 0.1 mm, was cut from an oriented spherical crystal in such a way that the easy axis of magnetization (crystallographic *c*-axis) was normal to the surface. It is seen that at RT (Fig. 7(*a*)) the sample is represented by a bright uniform circle in the center of the MOIF image surrounded by a dark ring representing, as expected, opposite directions of the stray field directly above and beside the sample, respectively.

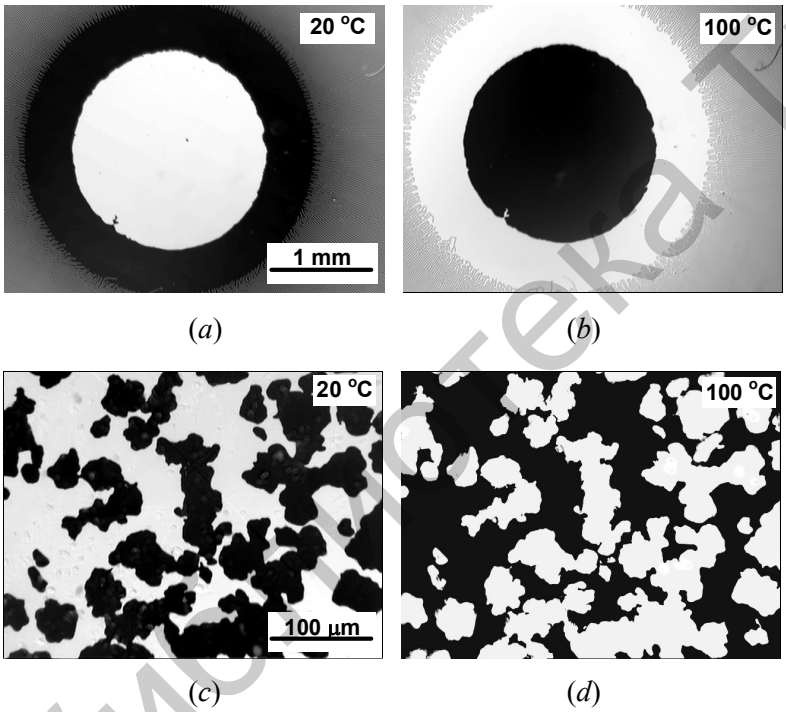

Fig. 7. Temperature-induced inversion of magnetization of saturated 2 mm disk $GdCo_3Cu_2$ single crystal [(*a*), (*b*)] and its 180° DS in demagnetized state [(*c*), (*d*)] as observed with MOIF at $T = 20$ and 100 °C. The compensation temperature T_{comp} is 90 °C

The whole picture is inverted at 100 °C, reflecting the change in dominance from the Gd sublattice magnetization to that of the 3*d* sublattice, on passing through the compensation point $T_{comp} = 90$ °C (Fig. 7(*b*)). Heating and cooling cycles were repeated many times without any signs of magnetization degradation. During temperature cycling, the MOIF shows its own unaffected DS at T_{comp}, demonstrating the zero magnetization state of the sample at this point.

The (*c*) and (*d*) images presented in Fig. 7 illustrate the effect of the temperature on the same sample in its multidomain state obtained by DC demagnetization. In these cases 180° magnetic DS typical of uniaxial crystals

is clearly observed at the temperatures below and above T_{comp}. Passing through the T_{comp} results in an inversion of the domain contrast. It is noteworthy that the configuration of the inverted DS reproduces the non-inverted one with a high degree of accuracy. This behavior suggests a unique possibility of producing a multipole magnet defined by artificially engineered periodic or aperiodic frozen DS configurations. In addition to the possibility of thermally switching between north and south pole configurations, such a magnet will also possess a very narrow (nanosize) transition zone width, equal to the domain wall width, between opposite poles. This feature is potentially important for applications in micro- and nano-electro-mechanical-systems (MEMS and NEMS). Furthermore, the possibility of changing the magnetization pattern (the position of transition zones) through the application of non-uniform temperature fields may also be exploited.

In the vicinity of T_{comp} the magnetization of the sample is near to zero, so the uniaxial MOIF demonstrates its own stripe DS practically unaffected by the sample under study (Fig. 8).

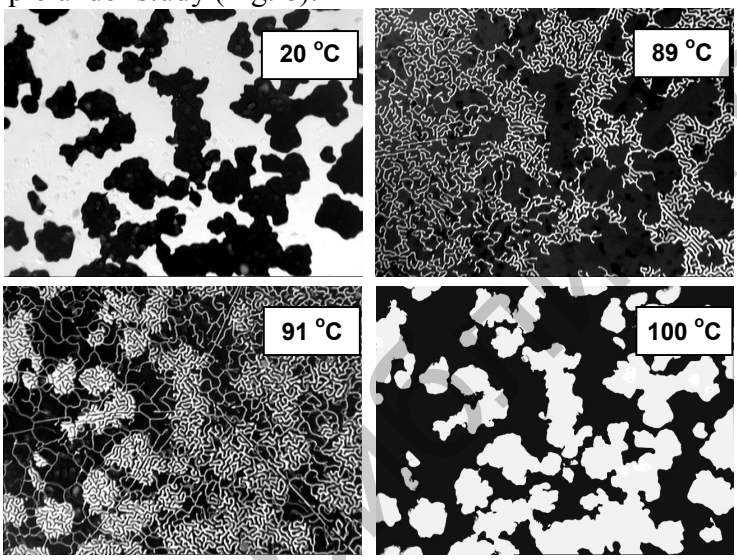

Fig. 8. Patterns produced by the uniaxial MOIF at the surface of $GdCo_3Cu_2$ at 20, 89, 91 and 100 °C. The compensation temperature T_{comp} is 90 °C

The effect of magnetization reversal with temperature may be demonstrated by heating the sample suspended by a thread in the field of a permanent magnet. On passing through the compensation point, the sample rotates by 180° and oscillates for some time in a decaying fashion, with a frequency depending on the moment of inertia of the system and rigidity due to both the sample and the suspension. This experiment serves to demonstrate a potential application of thermoreversible PM in resonance temperature sensors.As another demonstration of the possible use of thermoreversible

PM, we developed a modification of the recently described magnetic temperature sensors of the harmonic type [18–20]. A particular sensor proposed by Fletcher and Gerschenfeld [18] is comprised of three basic elements: the *signal element* (square loop soft magnetic tape producing detectable harmonics or detectable resonance frequency), the *bias element* (thin strip of semi-PM material), and the *modulation element* (soft magnetic material with a Curie temperature near the operating temperature for a given application). The modulation element changes its magnetic permeability with temperature leading, in turn, to a change of the biasing field of the adjacent semi-PM material acting on the signal element. As a result the magnetization harmonic spectrum of the signal element varies with temperature. This variation can be detected over a distance of several inches.

The same principle of temperature measurement may be implemented making use of one thermoreversible PM instead of two (bias and modulation) elements used in the original design [18]. When the signal element (nanocrystalline $Fe_{81}B_{13.5}Si_{3.5}C_2$ alloy in the form of a 40×5×0.02 mm thin strip in our case) is interrogated by an AC external field, the output signal spectrum in the absence of DC bias is presented by odd harmonics only (Fig. 9(*a*)). DC biasing by a small (100 mg) piece of $GdCo_3Cu_2$ PM placed at a distance of several millimeters from the strip results in the appearance of even harmonics with an amplitude comparable to that of the odd ones (Fig. 9(*b*)).

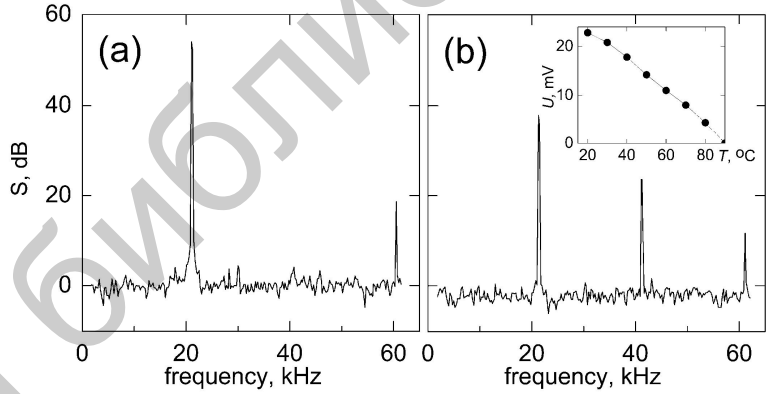

Fig. 9. Room temperature output signal spectrum of the sensor. (*a*) AC sinusoidal excitation at a frequency of 20040 Hz with zero bias (1st and 3rd harmonics); (*b*) same as (*a*) after DC biasing of the signal element by a thermo-reversible $GdCo_3Cu_2$ permanent magnet (2nd harmonic appeared). Inset: temperature dependence of the 2nd harmonic amplitude

The temperature dependence of the second harmonic amplitude presented in the inset of Fig. 9(*b*) is rather linear and completely reversible. It may be noted that the slope of the $M_r(T)$ curve of such a thermo-reversible PM is not changed when approaching the compensation point, thus allowing

clear zero reading, while ordinary thermomagnetic materials may suffer from magnetization "tails" near the Curie point.

To summarize this section, the present work has demonstrated that it is possible to have a combination of both ferrimagnetic compensation type behavior and magnetic hardness in $GdCo_{5-x}Cu_x$ alloys. Despite the relatively low values of magnetization, these alloys may be used as a special kind of PM, the magnetization of which can be reduced to zero or reversed by varying temperature. Experiments have been carried out to demonstrate the potential application of such a material in contactless temperature sensors as well as thermally controlled actuators. Other applications in magnetic MEMS are envisaged. Due to the resemblance of magnetic and physical properties of rare earth – transition metal alloys, other compositions with similar or better properties are likely to be found and alternative preparation methods such as powder metallurgy [12] or thin-film technologies [13] may be applicable.

3. Spin-reorientation materials

3.1. General remarks. Spin-reorientation is a special kind of magnetic transition of the order-order type. The most familiar example of a bulk material with spin-reorientation effect is cobalt, in which the direction of easy magnetization gradually rotates from the hexagonal crystal axis to the basal plane driven by a temperature change in the interval of 536 to 588 K. Spin-reorientation transitions (SRT) may be observed either under the temperature change (spontaneous SRT) or the change of the external magnetic field (induced SRT). The greatest variety of materials with SRT may be found among rare earth compounds – orthoferrites, garnet ferrites and intermetallic alloys of rare earth elements with cobalt and iron [21].

Thickness-driven transitions are additionally possible in thin and ultrathin films [22]. The strong thickness dependence of anisotropy in the latter systems originates from the characteristic contribution of interfaces.

Magnetic materials with SRT are of great fundamental interest, because their study promotes the development of both theory of magnetism and physics of phase transitions; moreover, there are promising indications of their potential use in a number of applications related to MEMS. Below we consider specific features of SRT in some uniaxial rare earth – cobalt intermetallic compounds of the RCo_5 family (hexagonal structural type $CaCu_5$) [6, 7].

3.2. Magnetic anisotropy and preferred axes and surfaces. The anisotropy energy of a ferromagnetic crystal is generally described in terms of anisotropy constants K_1, K_2, … multiplied by functions of angles having crystal symmetry. The energy of a hexagonal crystal is preferably expressed in polar coordinates by [21, 23, 24]

$$E_a^{hex} = K_1 \sin^2\theta + K_2 \sin^4\theta + K_3 \sin^6\theta + K_4 \sin^6\theta \cos 6\varphi + \ldots, \quad (1)$$

where the hexagonal axis is the polar axis and θ and φ the polar and azimuthal angles, the latter measured from an hexagonal *a*-axis.

Neglecting the anisotropy in the basal plane the case of cylindrical symmetry may be described with two first anisotropy constants as

$$E_a^{hex} = K_1 \sin^2\theta + K_2 \sin^4\theta . \qquad (2)$$

Depending on the sign and values of K_1 and K_2 (2) may describe the experimentally observed axes preferred by the magnetization (easy axes) or surfaces (easy planes or easy cones). Conditions for the minimum of (2) are

$$\partial E_a / \partial\theta = \sin\theta\cos\theta(K_1 + 2K_2 \sin^2\theta) = 0 ,$$

$$\partial^2 E_a / \partial\theta^2 = K_1 \cos^2\theta - K_2 \sin^2\theta + 6K_2 \sin^2\theta\cos^2\theta - 2K_1 \sin^4\theta > 0.$$

Minimization shows that the magnetization vector may be oriented either along the *c*-axis ($\sin\theta = 0$), or in the basal plane ($\cos\theta = 0$); also possible is angular (cone) structure ($\sin^2\theta = -K_1/2K_2$). Each of these solutions is thermodynamically stable for definite relations between the K_1 and K_2 constants:

$$\theta = 0,\ K_1 > 0 \text{ (easy axis);}$$

$$\theta = \pi/2,\ K_1 + 2K_2 \le 0 \text{ (easy -plane);}$$

$$\theta = \arcsin\sqrt{K_1 / 2K_2},\ K_1 + 2K_2 \ge 0,\ K_1 \le 0 \text{ (easy cone).}$$

For the case of $K_1 > 0$ and $K_1 < -2K_2$ minima for easy axis and easy plane states coexist (Fig. 10(*a*)). Easy axis minimum is absolute and that of easy plane metastable if $K_1 > -K_2$, while easy plane absolute minimum and metastable easy axis are observed when $K_1 < -K_2$.

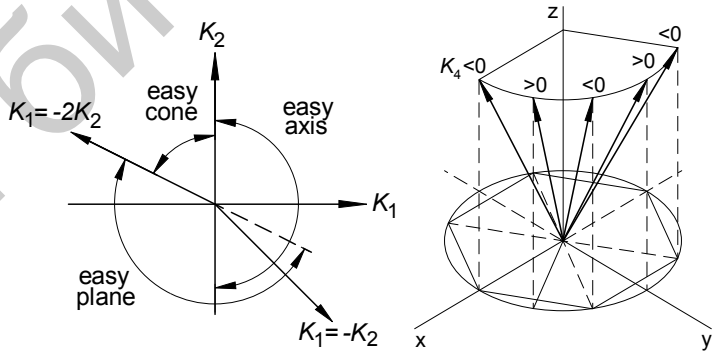

(*a*) (*b*)

F i g . 10. (*a*) The preferred directions of magnetization in an uniaxial crystal with cylindrical symmetry depending on the sign and value of anisotropy constants K_1 and K_2. (*b*) The preferred directions of magnetization vector lying on the preferred cone of a hexagonal crystal depending on the sign of anisotropy constant K_4The anisotropy in the

basal plane is taken into account by the fourth term on the right side of Eq. (1). The directions of preferred magnetization in the basal plane are defined by the sign of the anisotropy constant K_4 as illustrated in Fig. 10(*b*). For most hexagonal crystals the anisotropy in the basal plane is rather low thus making its experimental evaluation difficult.

3.3. Experiment. An instrument to monitor the changes of the easy magnetic axis of a sample during spontaneous SRT was constructed. In this instrument the sample is free to rotate continously aligning its easy axis with an external magnetic field produced by a permanent magnet (PM) (Fig. 11). The construction is similar to that described earlier [25] with the difference in the sample support.

Depending on the shape of the PM the dependence of the horizontal $B_z(z)$ field component near the lateral XZ side may be either saddle-shaped with two maxima near the PM edges or bell-shaped. For the latter case (Fig. 11(*b*)) a position may be found such that the sample will be stable against displacements along *x*- and *z*-directions. Simultaneous stability along *y*-direction is prohibited by the Earnshaw theorem, but in this direction the sample is constrained by the suspension. As a result magnetic self-centering of the sample occurs making unnecessary the use of a mechanical bearing. The field produced by the NdFeB magnet in the region of the sample is of the order of 0.2…0.4 T.

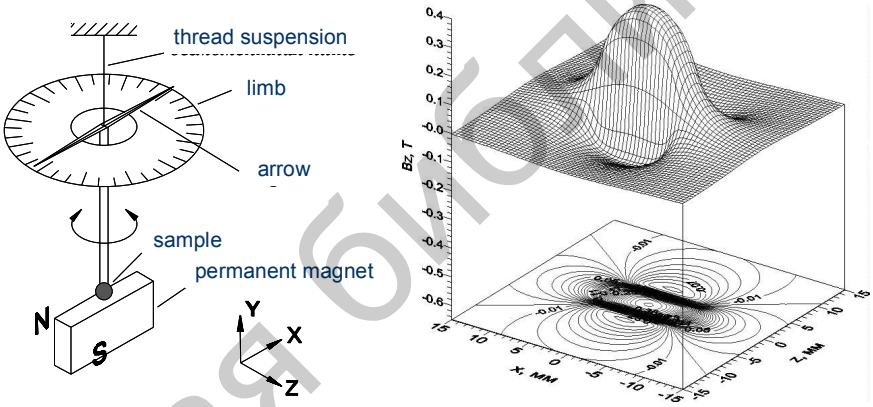

(*a*) (*b*)

Fig. 11. (*a*) Experimental determination of the easy axis direction changes during SRT with the sample self-centered in the field of a PM. (*b*) bell-shaped distribution of the B_z field component at a distance of 0.5 mm from the prismatic NdFeB magnet having dimensions 10×10×5 mm magnetized along *z*-axis

Fig. 12 illustrates the magnetic structure observed with the aid of the magneto-optic imaging film at the basal plane of the $DyCo_{5.2}$ single crystal. The temperature of 328 K corresponds to the early stage of the SRT. The deviation of the magnetization vectors from the plane of observation at this temperature is small, correspondingly the contrast of the picture is low. It becomes higher with heating (see images taken at 338 and 350 K) and achieves the maximum at 360 K. Note should be taken that the visually observed DS realignment proceeds very smoothly and manifests itself only in a gradual change of the image contrast without perceptible jumps of the Barkhausen type. Calibration of the image and its processing with a special software makes it possible to quantify the normal component of the field at the surface of the sample. The temperature dependence of this field component is plotted in Fig. 13(*a*) together with the magnetometer measurements.

In addition, shown in Fig. 13(*b*) is the temperature dependence of easy magnetization directions for the related quaternary alloys $Nd(Co_{.37}Al_{.08}Fe_{.05})_5$ and $Nd(Co_{.32}Al_{.12}Fe_{.06})_5$, which belong to the same family of hexagonal compounds crystallizing in the $CaCu_5$-type structure [26–27] and also are characterized by the existence of the easy plane – easy axis SRT. The presented data show that the SRT for these alloys occurs over a quite wide range in temperature. This result indicates that the magnetic moments do not tilt abruptly from a planar orientation to the axial one at T_{SRT}, but that they rotate continuously with temperature [28–29]. Thus the observed SRT appears to be a second order transition.

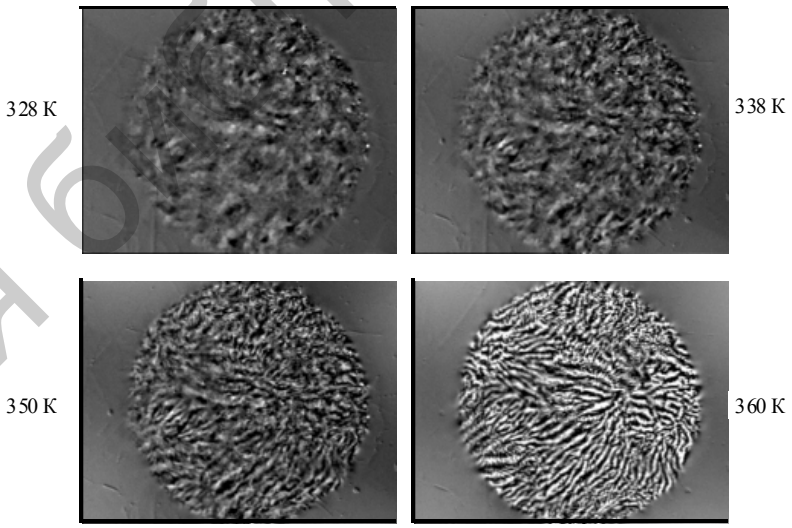

Fig. 12. Change of the normal stray field component at the basal plane of $DyCo_{5.2}$ single crystal as observed by a magneto-optic imaging film during easy plane to easy axis SRT

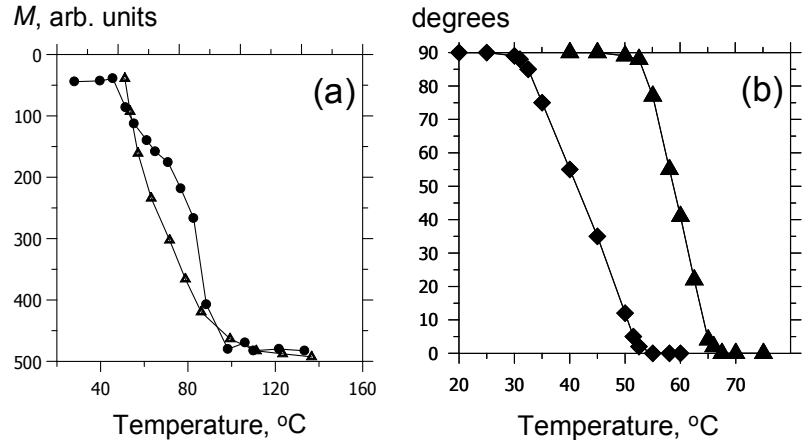

Fig. 13. (*a*) Temperature dependence of the normal field component magnitude at the basal plane of $DyCo_{5.2}$ obtained by image processing (circles) in comparison with magnetometer measurements (triangles). (*b*) Temperature dependence of easy magnetization directions for $Nd(Co_{.37}Al_{.08}Fe_{.05})_5$ (squares) and $Nd(Co_{.32}Al_{.12}Fe_{.06})_5$ single crystals (triangles)

This conclusion is further confirmed by the absence of noticeable Barkhausen jumps during the SRT observed at higher optical resolution provided by the use of polar Kerr effect (Fig. 14).

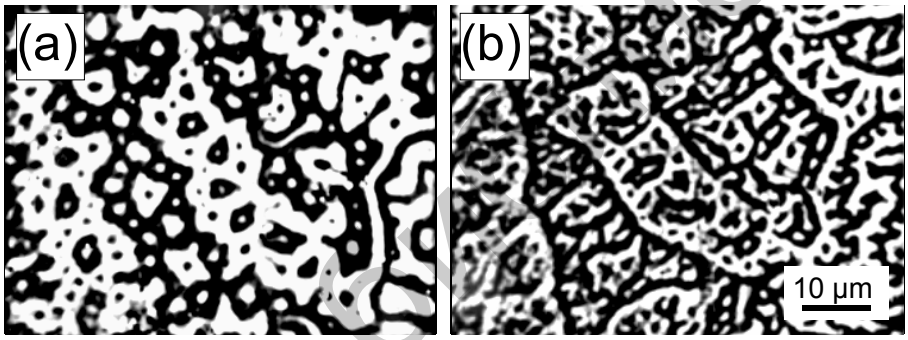

Fig. 14. Initial stage of DS realignment in $DyCo_{5.2}$ during cooling. (*a*) 80 °C, uniaxial anisotropy. (*b*) 65 °C, angular easy cone phase

In fact, the DS with clearly pronounced $L3$ and $L6$ symmetry elements indicating the easy cone anisotropy modulated by the sixfold basal plane anisotropy (Fig. 15(*a*)) is forming itself by homeomorphic (i.e. continuous) transformation from an isotropic structure. As for the DS in the easy plane state, it is comprised of irregular 180° domains elongated in the direction of *b*-axis in the basal plane (Fig. 15(*b*)). Rotation of the external magnetic field in the plane of the sample results in consecutive DS realignment by 60°-steps reflecting the hexagonal symmetry of the material (Fig. 15(*c*)).

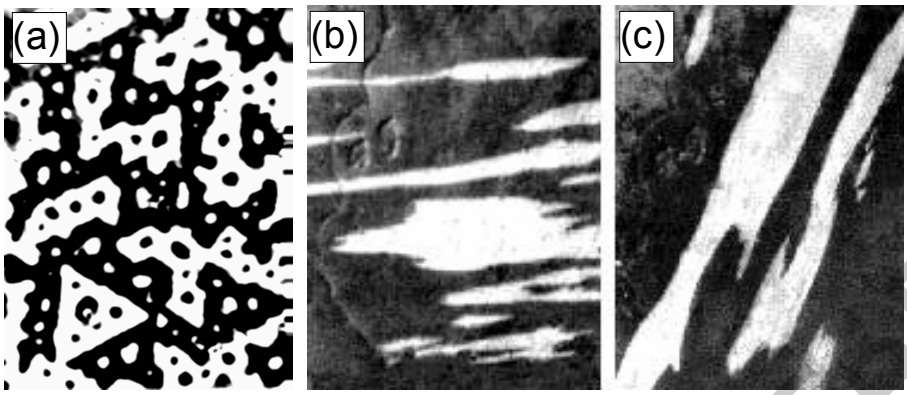

Fig. 15. (*a*) DS on the basal plane of $DyCo_{5.2}$ at 45 °C (easy cone anisotropy) demonstrating the L3 and L6 symmetry elements. (b)…(c) – 60-degree reorientation of 180° magnetic domains in the easy plane state of $DyCo_{5.2}$ at T=293 K caused by the external field ($\mu_0 H_e \sim 50$ mT) rotation in the basal plane of the sample

The easiness of magnetic moment rotation in the plane of the sample means that the anisotropy in the basal plane of the crystal is low though measurable. At the same time the magnetization rotation in the direction of unique hard axis (*c*-axis of the crystal for the easy plane state) requires high external fields of the order of anisotropy field, H_A. Applying field along the hard magnetic axis results in magnetization rotation characterized by an anhysteretic magnetization curve with constant susceptibility $\chi_{rot} = (\mu_0 M_s)^2 / 2K_1$ [7]. For $DyCo_5$ and a number of other high anisotropy rare earth – transition metal intermetallics the value of χ_{rot} in the hard direction is much smaller than the susceptibility due to domain wall motion χ_{dw} in fields parallel to the easy magnetic axis.

3.4. Resume. Large difference between the values of magnetic susceptibility in two mutually perpendicular directions and their reversible change by 90° due to the effect of SRT make it possible to use the latter in a number of applications based on the magnetic flux changeover – temperature controlled magnetic switches. An example of such a switch is shown in Fig. 16.

This switch is composed of two magnetically soft yokes having a gap filled with SR material. A permanent magnet (NdFeB) produces a magnetic flux in the yokes with a path dependent on the magnetic state of the SR material. The arrows show the magnetic flux path switching with the changeover of the easy axis direction due to SRT. This working principle may be used in a number of devices; in particular, a thermomagnetic generator on $Nd_{1-x}Dy_xCo_5$ displaying SRT was proposed by Ohkoshi and Kobayashi [30].

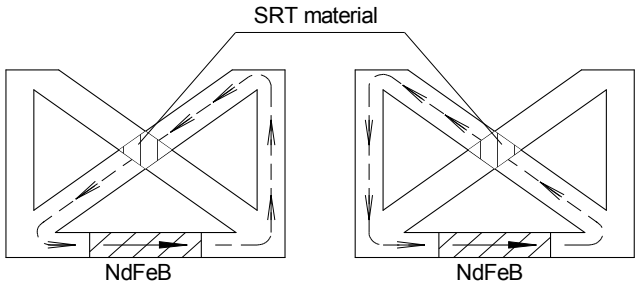

F i g . 16. Magnetic circuit topology of a thermomagnetic switching element on the base of a material with spin-reorientation transition from easy axis to easy plane state

SRT is also frequently occurring in rare earth intermetallic RFe_2 alloys with cubic Laves structure. These alloys are of interest on account of their giant magnetostriction [1, 2, 7]. Recently giant magnetostrictive films and exchange-coupled multilayers have been investigated for future MEMS purposes with reduction of the exciting field to a few oersteds [30–35]. Improvement of magneto-mechanical sensitivity near SRT was demonstrated for various modes of linear and nonlinear actuation of magnetostrictive unimorph [35] thus showing new horizons for application of SR materials.

4. Ferromagnetic shape memory alloys

4.1. General remarks. Ferromagnetic shape memory alloys (FSMA) have been shown to produce giant strain at least one order in magnitude larger than strain achievable with rare earth giant magnetostrictive materials [36–38]. Magnetically controlled strain in FSMA alloys is based on the reorientation of the twin structure of martensite under applied magnetic field. Physical properties and possible applications of these alloys were actively studied during the last decade [39–47]. The utilization of FSMA requires refined understanding of material behaviour, and particularly more detailed knowledge of the relations between coexisting and cooperating ensembles of ferromagnetic and martensitic domains.

The development of adequate quantitative theory of the interaction between martensitic and magnetic domain walls in real materials containing different crystal imperfections is a difficult problem. Its solution is restrained by the scarcity of necessary experimental data. Some results of the DS studies of FSMA obtained mainly by electron microscopy were reviewed recently [45–46]. Below we focus our attention on the experimental examination of the martensite and magnetic DS in Ni-Mn-Ga and Co-Ni-Ga alloys with the emphasis on the possibilites of optical methods.

4.2. Experimental. Polycrystalline Ni-Mn-Ga and Co-Ni-Ga alloys were prepared by arc melting in pure argon. The samples were homogenized for 100 hours at 800°C and water quenched. Single crystals were prepared by the Bridgman method described in detail elsewhere [48]. All samples were

checked by X-ray analysis. The characteristic temperatures of austenite-martensite transitions and Curie points were determined from the temperature variation of the AC susceptibility. All optical work was performed on a standard metallographic microscope refashioned to provide two-channel differential digital mode of observation in polarized light.

Unusual behaviour of the materials under study may be noticed during preparation of metallographic sections. Flat polished surfaces prepared on austenite samples acquire clearly pronounced relief after A→M transition into the martensite state. This relief delineates the martensite structure which may be observed by naked eye or in the microscope under ordinary bright light illumination (Fig. 17). Repeated heating (M→A) restores flatness. However if the flat surface is prepared on martensite samples it is not restored after a M→A→M cycle.

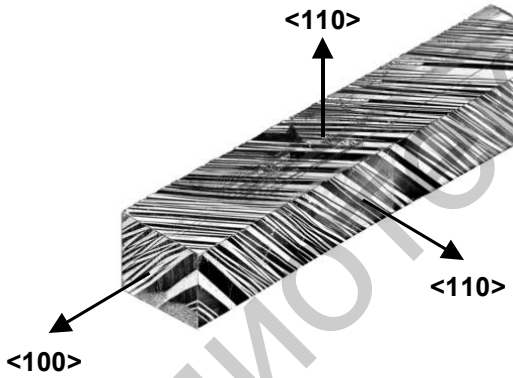

Fig. 17. Bright field image of the martensite relief of oriented $Co_{48}Ni_{22}Ga_{30}$ single crystal. Sample size 3×3×15 mm

Combination of deformation measurements with microstructural observations provides local information on the details of martensite variants behaviour during phase transitions (Fig. 18).

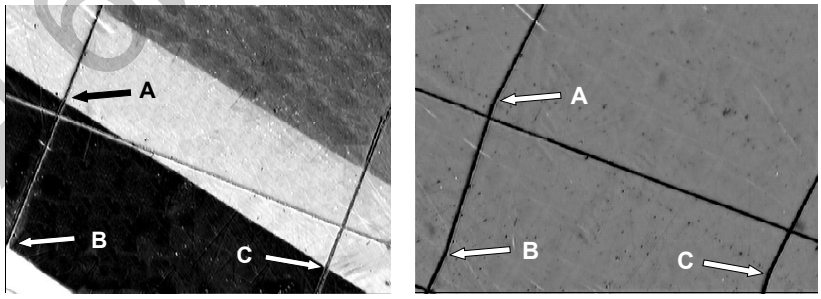

Fig. 18. Microstructure of $Ni_{2.16}Mn_{0.84}Ga$ at RT (martensite, left) and at T = 370 K (austenite, right) showing the deformation of initially rectangular diamond scratched reference grid. ×60

Observations in polarized light provide another way for the analysis of martensite structure. In this case optical contrast originates from anisotropic reflectance of the martensite phase and depends on the orientation of the *c*-axis with respect to the plane of light polarization (Fig. 19).

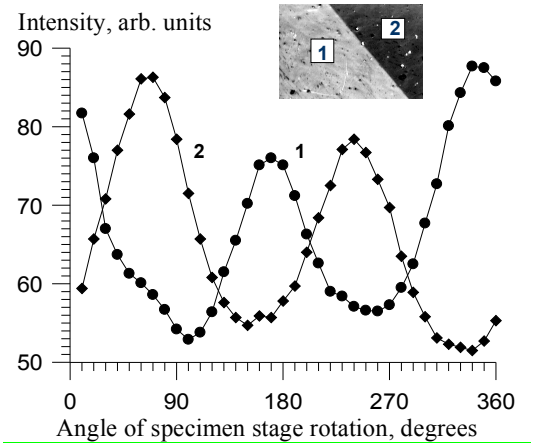

Fig. 19. Angular variation of the reflected light intensity for a $Ni_{2.16}Mn_{0.84}Ga$ sample. Curves 1 and 2 correspond to local measurements for variants 1 and 2. Curved intersections correspond to the condition of zero contrast between the variants

Fig. 19 demonstrates the dependence of the polarized light intensity reflected from adjacent martensite variants on the specimen angular position. It is seen that the optical contrast $C = (I_1 - I_2)/(I_1 + I_2)$ may be set to zero, be maximized or inverted by rotation of the sample on the microscope specimen stage. This specific feature helps to differentiate the images of martensite structure from those of magnetic domains revealed by Kerr effects.

4.3. Magnetic and martensite domain structure. It is well known that in bulk ferromagnetic samples diversified surface DS occurs in addition to main domains in order to minimize the magnetostatic stray fields when the magnetization **M** is not parallel to the sample surface. This surface DS of incidental interest disguises the structure of main domains important for the understanding of material behaviour.

Magneto-optic indicator films (MOIF) with mirror precoat, which were already successfully applied in the study of FSMA [44, 49] provide an interesting possibility of minimizing the camouflaging effect of secondary domains. To this end the MOIF is mounted on a gadget enabling to finely regulate the distance to the sample surface from zero to several tens of μm. At some selected distance the short-range stray fields from surface domains become negligibly small while the long-range fields from large main domains stay large enough to produce the image in the MOIF [14].

Shown in Fig. 20 is 3D view of magnetic 180° degree macrodomains on the {100} planes of $Ni_{2.3}Mn_{1.4}Ga$ single crystal obtained with the aid of MOIF. The observed macrodomains are running through the whole sample. Surface DS, as well as 90° modulation of **M** direction by martensite plates inside macrodomains in this case are out of vision.

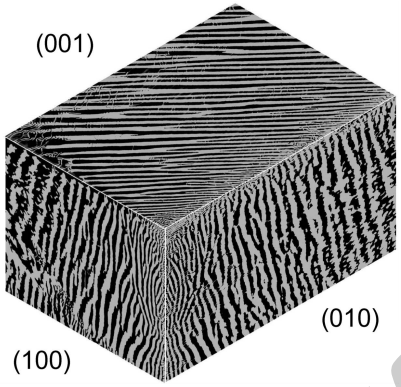

Fig. 20. 3D view of magnetic 180° macrodomains on the {100} planes of an oriented $Ni_{49}Mn_{29.7}Ga_{21.3}$ single crystal having dimensions of 1.2×1.5×2.5 mm

The above features are useful for quick inspection of the macro- and microstructure of crystals and estimation of the quality of single crystals. Figs. 21 and 22 demonstrate the examples of simultaneous observation of martensite and magnetic DS of FSMA. This was made possible making use of transparent MOIF without the Al mirror precoat.

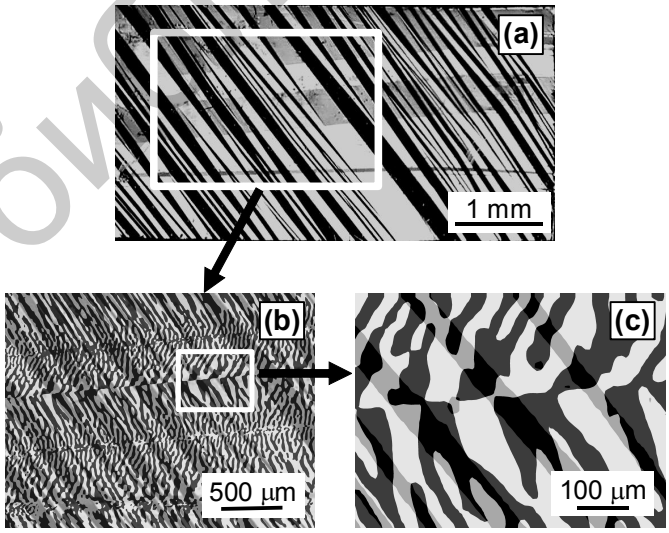

Fig. 21. (*a*) Martensite relief on the (110) surface of a $Co_{48}Ni_{22}Ga_{30}$ single crystal observed in the bright-field illumination mode. (*b*) The same sample as observed with the aid of a transparent MOIF. (*c*) Enlarged view of the rectangled area of (*b*).

In this case the martensite structure is seen through the MOIF which is transparent in the visible spectrum, whereas the magnetic Faraday image is formed by the light reflected from the MOIF – air interface and the sample surface. The enlarged view of Fig. 22 (*b*) shows the typical zigzag magnetic domains intersected by martensite twins.

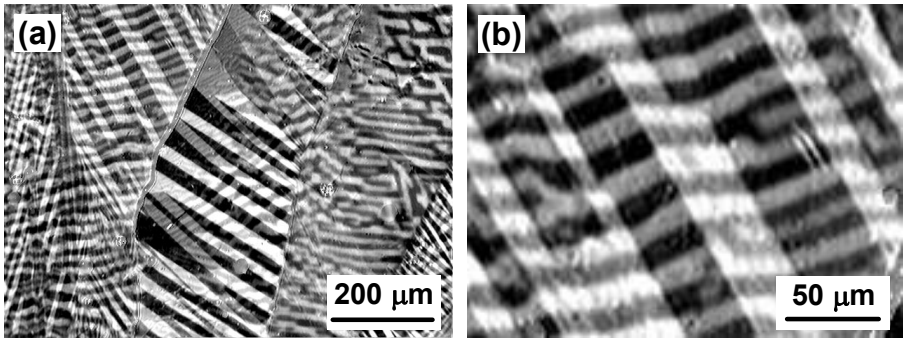

Fig. 22. (*a*) Simultaneous observation of martensite and magnetic DS of polycrystalline texturized $Ni_{2.16}Mn_{0.84}Ga$ ingot. (*b*) enlarged fragment of (*a*)

Fig. 23 shows the basic scheme of the martensite twins and main magnetic domains. Arrows show the direction of magnetization vectors **M**, while (+) and (-) signs indicate the appearance of surface magnetic poles.

From symmetry considerations only 180° magnetic domains may exist in twin plates because martensite possesses uniaxial magnetic anisotropy. Vector **M** is oriented along easy *c*-axes at angles of ±45° with respect to the twin boundaries. Due to magnetostatic coupling the 180° magnetic domains of neighbouring twins cooperate with each other forming continuous macrodomains running through the whole crystallite or single crystal sample and changing the direction of **M** by ±90° in a zigzag fashion at each intersection of the twin boundary.

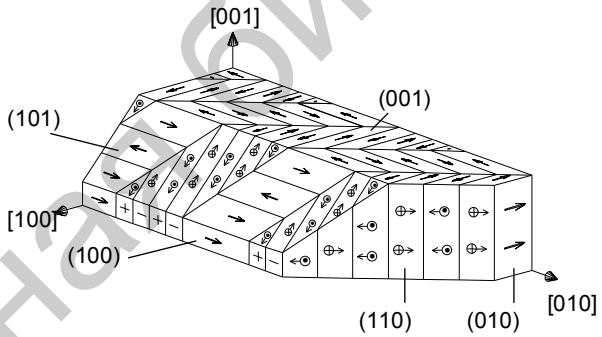

Fig. 23. Scheme of the magnetic substructure of martensite domains on different crystallographic planes

There is no experimental evidence of magnetic charges appearing at the intersection of magnetic domains with martensite boundaries, so it may be assumed that the 90° magnetization rotation at the twin wall is of the

Bloch type [7, 50], i.e. the normal component of the **M** vector remains constant during the 90° transition. Correspondingly the surface energy of the 90° Bloch wall bounded with the twin wall is $\gamma_{90°} = \gamma_{180°}/2 = 2\sqrt{AK_1}$ in usual notation.

The configuration of the domain walls on the sample surfaces depends on their crystallographic orientation and may be predicted from simple geometric considerations. The (001) plane is free of charges (Fig. 23); domain walls are oriented at $\varphi_{1,2} = \pm 45°$ with respect to the twin traces. For other planes these angles are different and are not necessary symmetric with respect to the twin traces on the surface (cf. Fig. 22 (*b*)). On (100) plane for odd twins **M** // (100), while for even ones **M** ⊥ (100), so in the latter case well-known surface subsidiary DS typical of uniaxial materials [50] should appear to minimize the stray fields. Various other combinations occur for arbitrary planes of observation.

In summary, the present study confirms the complicated character of the relationship between martensite and magnetic DS in FSMA. It is demonstrated that the combination of different complementary optical methods is useful in the study of this relationship. The versatility of optical methods is especially important in performing experiments under the action of external factors, in particular, for the study of materials behaviour in actual working conditions.

For the time being the most common usage of FSMA in linear motion actuators. Benefits of such actuators were found to be fast motion, high operating frequencies, high strains and damping abilities [51, 52] Operating temperatures of the present Ni-Mn-Ga FSMA range from –40 to 60°C; an increase to 120 °C is expected. A number of different types of actuators were developed by AdaptaMat Ltd [52]; among these is, for example, an actuator with the size of 11×23×21 mm producing a maximum stroke of 0.6 mm in a frequency range from DC to 1000 Hz. Thin film, composite and spring actuators are under development [53–56]. Different kinds of reverse operations like energy generation, position-, velocity and acceleration sensors can be implemented with FSMA [57]. Mechanical straining of FSMA may also be used for voltage or power generation [58].

This work was performed within the Federal Target Program "Research and Research-Pedagogical Personnel of Innovation Russia for 2009-2013".

References

1. Jiles D.C. and Lo C.C.H. The role of new materials in the development of magnetic sensors and actuators // Sensors and Actuators. 2003. A106. P. 3–7.
2. Jiles D.C. Recent advances and future directions in magnetic materials // Acta Mater. 2003. V. 51. P. 5907–5939.

3. McHenry M.E. and Laughlin D.E. Nano-scale materials development for future magnetic applications // Acta Mater. 2000. V. 48. P. 223–238.
4. Herzer G. Magnetic materials for electronic article surveillance // J. Magn. Magn. Mater. 2003. V. 254–255, 598–602.
5. Reyne G., Delamare J., Cugat O., in: Cugat O. (Ed.). Microactionneurs Electromagnétiques – MAGMAS. Paris, Hermes Science Publications. 2002.
6. Parker R.J. Advances in Permanent Magnetism. Wiley-Interscience Publ., New York. 1990.
7. O'Handley R.C. Modern Magnetic Materials: Principles and Applications. Wiley, New York. 2000.
8. Nesbitt E.A., Wilens R.H., Sherwood R.C., Buehler F., and. Wernick J.H. New permanent magnet materials // Appl. Phys. Let. 1968. V. 12. P. 361.
9. Ermolenko A.S. and Korolyov A.V. Giant coercive force and certain features in the magnetization of bulky single crystals of the intermetallic compounds $Sm(Co_{1-x}Ni_x)_5$. // Sov. JETP Lett. 1975. V. 21. P. 15–17.
10. Tellez-Blanco J.C., Grossinger R., Sato Turtelli R. Structure and magnetic properties of $SmCo_{5-x}Cu_x$ alloys. // J. Alloys. Comp. V. 281(1). P. 1–5.
11. Grossinger R., Tellez-Blanco J.C., Sato Turtelli R.S., Hauser R., Reiterer K., Sassik H., Chouteau G. Determination of the magnetic viscosity in $SmCo_{5-x}Cu_x$ alloys by pulsed-field method // Physica B: Cond. Matter. 2001. B294–295. P. 194–198.
12. Sagawa M., Yamaguchi W. and Henmi Z. Temperature-sensitive Nd-Co compounds produced by powder metallurgy // J. Appl. Phys. 1981. V. 52. P. 2520–2522.
13. Hasegawa R. and Taylor R.C. Magnetization of amorphous Gd-Co-Ni films // J. Appl. Phys. 1975. V. 46. P. 3606–3608.
14. Grechishkin R.M., Goosev M.Yu., Ilyashenko S.E. and Neustroev N.S. High resolution sensitive magnetooptic ferrite garnet films with planar anisotropy // J. Magn. Magn. Mater. 1996. V. 157–158. P. 305–306.
15. Ermolenko A.S., Korolyov A.V. and Shur Ya.S. $SmCo_5$ crystals with magnetic energy 32 million Gauss-Oersted // Sov. JETP Lett. 1973. V. 17. P. 499.
16. Katayama T., Ohkoshi M., Koizumi Y., Shibata T., Tsushima T. Magnetization reversal in $GdCo_5$ single crystals // Appl. Phys. Lett. 1976. V. 28. P. 635–637.
17. Fidler J., Schrefl T., Hoefinger S., Hajduga M. Recent developments in hard bulk materials. J. Phys.: Condens. Matter. 2004. V. 16. S455-S470.
18. Fletcher R. and Gerschenfeld N.A. Remotely interrogated temperature sensors based on magnetic materials // IEEE Trans. Magn. 2003. V. 36. P. 2794–2795.
19. Ong K.C. and Grimes C.A. Magnetically soft higher order harmonic stress and temperature sensors // IEEE Trans. Magn. 2000. V. 39. P. 3414–3416.
20. Ong K.C., Grimes C.A., Robbins C.L. and Singh R.S. Design and application of a wireless, passive, resonant-circuit environmental monitoring sensor // Sensors and Actuators. 2001. V. A93. P. 33–43.
21. Belov K.P., Zvezdin A.K., Kadomtsev A.M., Levitin R.Z. Orientational transitions in rare earth magnets. Nauka, Moscow. 1979 (in Russian).
22. Millev Y.T., Oepen H.P. and Kirschner J. Influence of external field on spin reorientation transitions in uniaxial ferromagnets. I. General analysis for bulk and thin-film systems // Phys. Rev. B. 1998. V. 57(10). P. 5837–5847.

23. Carr W.J. Secondary effects in Ferromagnetism, in: Handbuch der Physik. XVIII/2 (Berlin, Springer, 1966). P. 274-340.
24. Zijlstra H., Experimental Methods in Magnetism. North-Holland, Amsterdam. 1967. Chap. 5.
25. Antonini B., D'Angelo S., Foco A., Maturi B. and Paroli P. An easy axis monitor for the detailed study of spin transitions. Application to $ErFeO_3$ and $Er_3Fe_5O_{12}$ // IEEE Trans. Magn. 2000. V. 18. P. 1562–1564.
26. Banerjee D., Bahadur D., Suresh K.G. and Nigam A.K. Effect of Cu substitution on the structural and magnetic properties of $DyCo_{5-x}Cu_x$ // Phys. B: Cond. Matter. 2006. V. 378–380. P. 1091–1092.
27. Miletic G.I. and Blazina Z. Electronic structure and spin magnetic moments in the $DyCo_{5-x}Al_x$ system // J. Magn. Magn. Mater. 2004. V. 284. P. 312–320.
28. Klosek V., Zlotea C. and Isnard O. Structural and magnetic properties of hexagonal $DyCo_4M$ compounds (M = Al, Ga) // J. Phys.: Condens. Matter. 2003. V. 15. P. 8327–8337.
29. Kuz'min M.D. On the gradual character of the first-order spin reorientation transition in $DyFe_{11}Ti$ // J. Appl. Phys. 2000. V. 88(12). P. 7217–7222.
30. Ohkoshi M. and Kobayashi H. Rotational-type spin reorientation in $Nd_{1-x}Dy_xCo_5$ and its application to thermomagnetic generator // IEEE Trans. Magn. 1977. V. 13(5). P. 1158–1160.
31. Quandt E., Holleck H. Materials development for thin film actuators // Microsyst. Technol. 1995. V. 1. P. 178–184.
32. Quandt E., Ludwig A., Lord D.G., Faunce C.A. Magnetic properties and microstructure of giant magnetostrictive TbFe/FeCo multilayers // J. Appl. Phys. 1998. V. 83(11). P. 7267–7269.
33. Tiercelin N., Preobrazhensky V., Pernod P., Legall H. and J. Ben Youssef, Sub-harmonic excitation of a planar magnetomechanical system by means of giant magnetostrictive film // J. Magn. Magn. Mater. 2000. V. 210. P. 302–308.
34. Ben Youssef J., Tiercelin N., Petit F., Le Gall H., Preobrazhensky V. and Pernod P. Statics and dynamics in giant magnetostrictive Tb_xFe_{1-x}-$Fe_{0.6}Co_{0.4}$ multilayers for MEMS // IEEE Trans. Magn. 2002. V. 38. P. 2817–2819.
35. Tiercelin N., Ben Youssef J., Preobrazhensky V., Pernod P. and Le Gall H. Giant magnetostrictive superlattices: from spin reorientation transition to MEMS. Static and dynamical properties // J. Magn. Magn. Mater. 2002. V. 249(3). P. 519–523.
36. Ullakko K., Huang J.K., Kantner C., O'Handley R.C. and Kokorin V.V. Large magnetic-field-induced strains in Ni_2MnGa single crystals // Appl. Phys. Lett. 1996. V. 69. P. 1966–1968.
37. O'Handley R.C. Model for strain and magnetization in magnetic shape-memory alloys // J. Appl. Phys. 1998. V. 83. 3263–3270.
38. Marioni M.A., O'Handley R.C., Allen S.M., Hall S.R., Paul D.I., Richard M.L., Feuchtwanger J., Peterson B.W., Chambers J.M. and Techapiesancharoenkij R. The ferromagnetic shape-memory effect in Ni–Mn–Ga // J. Magn. Magn. Mater. 2005. V. 290–291. P. 35–41.
39. Pan Q. and James R.D. Micromagnetic study of Ni_2MnGa under applied field (invited) // J. Appl. Phys. 2000. V. 87(9). P. 4702–4706.
40. Wuttig M., Li J. and Craciunescu C. A new ferromagnetic shape memory alloy system // Scr. Mater. 2001. V. 44. P. 2393–2397.

41. Wuttig M., Li J., Craciunescu C. New ferromagnetic and functionally graded shape memory alloys // J. Optoelectr. Adv. Mater. 2003. V. 5. P. 139–146.
42. Pasquale M., Sasso C.P., Besseghini S. and Chernenko V. Field and temperature induced giant strain in single crystal Ni-Mn-Ga // IEEE Trans. Magn. 2001. V. 37(4). P. 2669–2671.
43. Chernenko V.A., Zagorodnyuk S.P., L'vov V.A., O'Handley R.C., Kono Y. Magnetization curves fior tetragonal martensites: experiments and modelling // J. Appl. Phys. 2006. V. 99. P. 103906.
44. Korpusov O.M., Grechishkin R.M., Koledov V.V., Khovailo V.V., Takagi T., Shavrov V.G. Simultaneous magnetooptic observation and thermomagnetic analysis of phase transitions in shape-memory Ni-Mn-Ga alloys // J. Magn. Magn. Mater. 2004. V. 272–276. P. 2035–2037.
45. Grechishkin R.M., Lograsso T.A., Schlagel D.L., Koledov V.V., Zalyotov A.B., Chigirinsky S.A. Martensite and magnetic domain structure in ferromagnetic shape memory single- and polycrystals. In: Proc. Third Moscow Intern. Symp. Moscow, MSU. 2005. P. 207–211.
46. Heczko O. Magnetic shape memory effect and magnetization reversal // J. Magn. Magn. Mater. 2005. V. 290–291. P. 787–794.
47. Ge Y., Heczko O., Soderberg O., Hannula S.-P. and Lindroos V.K. Investigation of magnetic domains in Ni–Mn–Ga alloys with a scanning electron microscope // Smart Mater. Struct. 2005. V. 14. P. S211–S215.
48. Schlagel D.L., Wu Y.L., Zhang W. and Lograsso T.A. Chemical segregation during bulk single crystal preparation of Ni-Mn-Ga ferromagnetic shape memory alloys // J. Alloy Comp. 2000. V. 312. P. 77–85.
49. Sozinov A., Ezer Y., Kimmel G., Giller D., Wolfus Y., Yeshurin Y., Ullakko K. and Lindroos V.K. // J. Phys. IV France. 2001. V. 11. P. Pr8-311–Pr8-316.
50. Hubert A. and Schäfer R. Magnetic Domains. The Analysis of Magnetic Microstructures. New York: Springer. 1998.
51. Aaltio I. and Ullakko K. Magnetic shape memory (MSM) actuators. Actuator 2000. Germany. Bremen. 2000. P. 527–530.
52. http://www.adaptamat.com
53. Wada T., Lee R.C.C., Chen S.H.H., Kusaka M. and Taya M. Design of spring actuators made of ferromagnetic shape memory alloy and composites // Proc. SPIE. 2003. V. 5054. P. 125–134.
54. Liang Y., Taya M., Kuga Y. Design of membrane actuators based on ferromagnetic shape memory alloys composite for the synthetic jet actuator. Proc. SPIE 5390. 2004. P. 268–275.
55. Kohl M., Liu Y., Krevet B., Durr S. and Ohtsuka M. SMA microactuators for microvalve applications // J. Phys. IV France. 2004. V. 115. P. 333–342.
56. Kohl M., Hoffmann S., Liu Y., Ohtsuka M. and Takagi T. Optical scanner based on a NiMnGa thin film microactuator // J. Phys. IV France. 2003. V. 112. P. 1185–1188.
57. 10th Intern. Conf. on New Actuators ACTUATOR-2006. Bremen, Germany. 14–16 June 2006.
58. Suorsa I., Tellinen J., Ullakko K. and Pagounis E. Voltage generation by mechanical straining in magnetic shape memory material // J. Appl. Phys. 2004. V. 95. P. 8054–8058.

ТЕРМОУПРАВЛЯЕМЫЕ МАГНИТНЫЕ МАТЕРИАЛЫ ДЛЯ МИКРОЭЛЕКТРОМЕХАНИЧЕСКИХ СИСТЕМ (обзор)

М. С. Кустов[1], Г. А. Лебедев[2], С. Е. Ильяшенко[3], Д. В. Друина[1], О. В. Гасанов[1], С. А. Чигиринский[4],О. М. Корпусов[5], А. Б. Залётов[5], Р. М. Гречишкин[1]

[1] Тверской государственный университет
[2] CEA, LETI, MINATEC Campus, Grenoble, France
[3] Тверской государственный технический университет
[4]ЗАО предприятие ОСТЕК
[5] Тверская государственная медицинская академия

Рассматриваются три новых разновидности магнитных материалов (термоуправляемые постоянные магниты, спин-переориентационные соединения и ферромагнитные сплавы Гейслера с памятью формы), представляющие интерес для будущих применений в микроэлектромеханических системах. Подчёркивается роль исследований доменной структуры (ДС) для понимания особенностей магнитного поведения этих материалов. Магнитные свойства и ДС высококоэрцитивных сплавов $GdCo_{5-x}Cu_x$, обладающих точкой компенсации подрешёток Gd и 3*d*–элементов описываются в связи с их применением в качестве термоуправляемых постоянных магнитов. Изменения типа ДС при спин-переориентационном переходе от одноосного состояния к состоянию с анизотропией «лёгкая плоскость» рассматриваются на примере интерметаллического соединения $DyCo_5$. Магнитоупорядоченные сплавы Гейслера (Ni-Mn-Ga, Co-Ni-Ga) с эффектом памяти формы характеризуются кооперативными взхаимодействиями между мартенситной и магнитной ДС. Приводятся примеры возможных применений рассматриваемых материалов в устройствах, связанных с микроэлектромеханическими системами (МЭМС).

Ключевые слова: *термоуправляемые магниты, магнитотвёрдые материалы, редкоземельные соединения, спиновая переориентация, сплавы с памятью формы, магнитная доменная структура, магнитооптические индикаторные плёнки*

Об авторах:

КУСТОВ Михаил Сергеевич – кандидат физ.-мат. наук, старший научный сотрудник ТвГУ, 170100, г. Тверь, ул. Желябова, 33;

ЛЕБЕДЕВ Гор Андреевич – аспирант CEA–LETI–MINATEC Campus, Гренобль, Франция;

ИЛЬЯШЕНКО Светлана Евгеньевна – кандидат физ.-мат. наук, доцент кафедры технологии металлов и материаловедения ТГТУ, *e-mail:* SvIlyashenko@yandex.ru;

ДРУИНА Дарья Викторовна – магистрант кафедры прикладной физики ТвГУ;

ГАСАНОВ Олег Валерьевич – магистрант кафедры прикладной физики ТвГУ;

ЧИГИРИНСКИЙ Сергей Анатольевич – кандидат физ.-мат. наук, ведущий специалист отдела микроэлектроники ЗАО предприятия ОСТЕК (Москва), *e-mail:* sergey.chigirinsky@ostec-smt.ru;

КОРПУСОВ Олег Михайлович – кандидат физ.-мат. наук, доцент кафедры физики ТГМА;

ЗАЛЁТОВ Алексей Борисович – кандидат физ.-мат. наук, доцент кафедры физики ТГМА;

ГРЕЧИШКИН Ростислав Михайлович – кандидат физ.-мат. наук, профессор кафедры прикладной физики ТвГУ, *e-mail:* rostislav.grechishkin@tversu.ru.